# Crack Detection in a Rotor Dynamic System by Vibration Monitoring—Part I: Analysis

**Itzhak Green**
Georgia Institute of Technology,
GWW School of Mechanical Engineering,
Atlanta, GA 30332
Fellow ASME

**Cody Casey**
Schlumberger,
14910 Airline Road,
Rosharon, TX 77583

*Many practical rotor dynamic systems contain shaft/rotor elements that are highly susceptible to transverse cross-sectional cracks due to fatigue. The early detection of mechanical malfunction that can be provided by an effective vibration monitoring system is essential. Two theoretical analyses, global and local asymmetry crack models, are utilized to identify characteristics of the system response that may be directly attributed to the presence of a transverse crack in a rotating shaft. A model consisting of an overhung whirling rotor is utilized to match an experimental test rig. A 2X harmonic component of the system response is shown to be the primary response characteristic resulting from the introduction of a crack. Once the unique characteristics of the system response are identified, they serve then as target observations for the monitoring system.*
[DOI: 10.1115/1.1789514]

## 1 Introduction

As rotating machinery is designed to operate at higher mechanical efficiency; operating speed, power, and load are increased as weight and dimensional tolerances are decreased. The result is a significantly increased level of operating stress in modern rotating machinery. As a consequence, many practical rotordynamic systems contain shaft/rotor elements that are highly susceptible to transverse cross-sectional cracks due to fatigue. To accurately predict the response of a system to the presence of a transverse crack, an appropriate crack model is essential. Once the crack is included in the system model, unique characteristics of the system response can be identified and attributed directly to the presence of the crack. These predicted indicators then serve as target observations for monitoring systems.

A significant amount of research involving the prediction of the response of shaft/rotor systems to the presence of a transverse crack, and the detection of transverse cracks in rotating shafts by vibration monitoring, has been completed in the last 30 to 40 years. This work is an extension of a body of research focused on a flexibly mounted rotor (FMR) mechanical face seal system [1]. The dynamics of the FMR mechanical face seal system have been extensively investigated [2–5]. In Ref. [2] the coupled dynamics of the seal and shaft is investigated including effects of shaft inertia and slenderness, fluid film, secondary seal, flexibly mounted rotating element, and an axial offset of the rotor center of mass. The steady-state response was investigated by implementing a complex extended transfer-matrix method. In Ref. [3] an experimental correlation is investigated between the presence of higher harmonic oscillations in the test rig system and seal face contact. The dynamics behavior of the FMR seal itself was investigated in Refs. [4] and [5]. Seal failure, diagnostics, control, and eventual performance restoration are extensively discussed in Refs. [6–10]. To achieve these goals it is imperative that failure characteristics of seal and shaft are well differentiated. The influence of a crack in a seal-driving shaft is the concern of this work.

An uncracked shaft has constant stiffness, and thus constant displacement under a fixed load, regardless of the angle of rotation. In a cracked shaft, the cracked portion of the cross section is not capable of supporting a tensile stress. Therefore the displacement, as a function of the stiffness, is minimum when the crack is closed and maximum when the crack is open. This opening and closing behavior, which is referred to as ''breathing,'' results in time-dependent stiffness coefficients in the equations of motion of the system, which is difficult to work with. Obtaining solutions usually requires making broad simplifying assumptions or some type of numerical approximation.

Systems in which static displacements and vibrational amplitudes remain very small result in a crack that remains essentially open regardless of the angle of rotation. This type of crack, which is essentially a local stiffness asymmetry, is referred to as a ''gaping'' crack. The analysis of systems containing a gaping crack is extremely useful since the response characteristics, or crack indicators, identified in the gaping crack analysis are also present in the analysis of systems containing a breathing crack. Furthermore, these indicators prove to be the most practical, in terms of implementation, in the detection of real cracks. Also, since the introduction of a crack into a rotating system, on the most basic level, results in a system with a stiffness asymmetry, the analysis of systems containing an asymmetry is fundamental to the study of the dynamics of cracked rotating systems.

The primary effect of the presence of a crack in a rotating shaft is clearly a local reduction in stiffness. This highly localized effect does not influence the stiffness of the regions of the rotor away from the cracked cross section. Regardless of the type of crack model used for analysis, the effective overall stiffness of the rotor is no longer symmetric. The analysis of the response of a rotor with designed-in asymmetry is therefore part of the fundamental basis for the analysis of the dynamics of shafts containing a transverse crack.

A free response of a two degree-of-freedom rotor with asymmetric moments of inertia [11] shows a range of shaft speeds in which the response is unstable. The appearance of a region of instability near the first natural frequency is confirmed in Ref. [12], as well as the $2X$ harmonic response in an analysis of a linearly asymmetric shaft. In Ref. [13] the $2X$ resonance is also predicted at approximately one-half of the first natural frequency. An intuitive explanation for the existence of a region of instability and a $2X$ harmonic response in shafts with dissimilar moments of inertia is given in Ref. [14]. It is important to note that for rotating systems, the terms ''natural frequency'' and ''whirl frequency'' are synonymous. Also, the term ''critical speed'' refers to a shaft speed for which one or more of the natural (whirl) frequencies of

Contributed by the International Gas Turbine Institute (IGTI) of THE AMERICAN SOCIETY OF MECHANICAL ENGINEERS for publication in the ASME JOURNAL OF ENGINEERING FOR GAS TURBINES AND POWER. Paper presented at the International Gas Turbine and Aeroengine Congress and Exhibition, Atlanta, GA, June 16–19, 2003, Paper No. 2003-GT-38659. Manuscript received by IGTI, October 2002, final revision, March 2003. Associate Editor: H. R. Simmons.

the system are equal to the shaft speed. Therefore the maximum $2X$ harmonic response occurs at shaft speeds that are approximately one-half of a critical speed, i.e., $\frac{1}{2}n_{cr}$.

In Ref. [15] a practical "hinge model" is developed that represents the crack as an additional flexibility in the direction perpendicular to the crack edge, for positive displacements in that direction. Similar displacement based breathing crack models have been utilized in Refs. [12,13,16–19]. In Ref. [20] the opening and closing of the crack is modeled as a step type function of the angle of rotation only. Other similar step and 1/rev continuous functions of the angle of rotation have been used to model the breathing behavior of the crack in Refs. [16–18,21–28].

The complicated system models resulting from the inclusion of a breathing crack model have been solved or approximated by a variety of methods. Analog computer simulations [12,15], Ritz basis functions based on the asymmetric solution [16], and numerical integration [13,17,18,20] have been used. Various transfer-matrix methods were employed as well [19,23,29]. Floquet theory stability analysis is performed in Refs. [21,27,30], and perturbation methods are utilized in Refs. [24,25].

The most significant result of the analysis of systems containing breathing crack models that is relevant to this work is the fact that the response characteristics due to a breathing crack model consist of the primary response characteristics of an asymmetric system plus some additional phenomena, in form of sub or higher harmonics [20,21,24,25,30–34]. The direction of the investigations into the response of rotating systems containing breathing crack models tends to focus on the $1X$ and $2X$ harmonic responses [17,23–25,33,34].

On the most basic level the introduction of a gaping crack results in a local system stiffness asymmetry that is time independent in a rotating coordinate frame. The additional flexibility introduced to the system by the presence of the crack is determined by methods such as finite element analysis or the Paris strain energy method [21,30]. The localization of the stiffness asymmetry is the key in this analysis.

In Refs. [21,30,33,34] the overall stiffness properties for their two and three degree-of-freedom systems is determined by conveniently placing the crack at the mid-span of the De-Laval rotor system. To arbitrarily place the crack at some location along the shaft in the system model, it is convenient to utilize a discrete representation of the system, such as a transfer-matrix method [29]. The presence of a gaping crack in the shaft of a rotating system tends to primarily affect the $1X$ synchronous response, and the $2X$ harmonics, which has a resonance at $\frac{1}{2}n_{cr}$.

In summary, the introduction of a gaping crack model into an existing system model has been shown to be a very effective method of obtaining reasonably accurate results from analysis, yet it avoids the inherent complexities of cracked shaft analysis due to breathing behavior. A discrete representation of the system allows the additional flexibility due to the crack to be placed arbitrarily along the axis of the shaft of the system. The $2X$ harmonic component of the system response is clearly the most practically implemented indicator for a monitoring and detection system. This work utilizes a global asymmetry crack model in a continuous representation of the system as well as a gaping crack model in a discrete representation of the system using a unique extended transfer-matrix formulation [2]. The theoretical analyses focus on the prediction of the behavior of the $2X$ component of the system response. For each crack model, free and forced response characteristics are investigated.

## 2 Global Asymmetry Crack Model

A shaft into which a transverse crack is introduced experiences a reduction in stiffness which, depending on the relative dimensions of the crack, can be quite small or quite large. As a first approximation we consider a shaft whose entire cross section is represented by the remaining uncracked cross section. Thus the resulting shaft is assumed to have an asymmetric cross section over its entire length. This is referred to as a global asymmetry crack model, which is the worst case in terms of the amplitude of the resulting response characteristics. (Such an analysis is useful by itself since many rotor dynamic systems contain designed-in asymmetric components.)

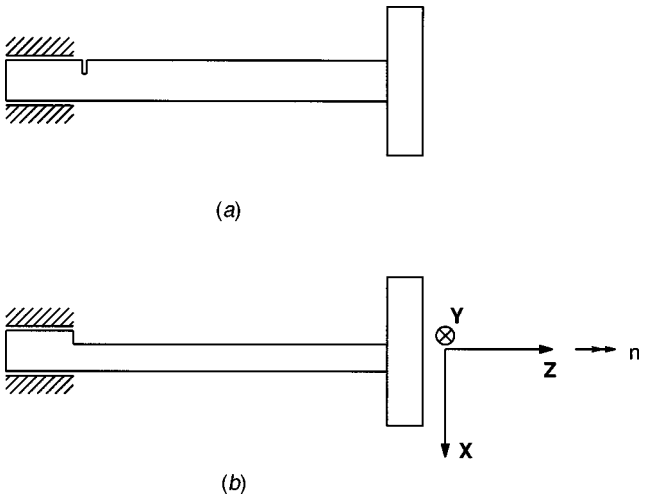


**Fig. 1 (*a*) Cracked system; (*b*) global asymmetry crack model**

In Fig. 1(*a*) the cross section of an overhung massless shaft with an attached rotor (which is a reasonable representation of the test rig system that is detailed in Ref. [35]) is shown to include a transverse crack. Figure 1(*b*) shows the same system including the global asymmetry crack model, which is essentially an asymmetric Euler-Bernoulli beam. Equations of motion for this system are derived in a rotating frame to avoid time-dependent stiffness coefficients. The $XYZ$ coordinate system rotates with the shaft, at shaft speed $n$, and is oriented such that the $X$ axis is perpendicular to the crack edge. The relationship between the rotating $XYZ$ coordinate system and the inertial $\xi\eta\zeta$ coordinate system is shown in Fig. 2. The equations of motion can be derived in the rotating $XYZ$ coordinate frame as detailed in Ref. [35], which is based upon the work in Ref. [36]. For the no damping case we have

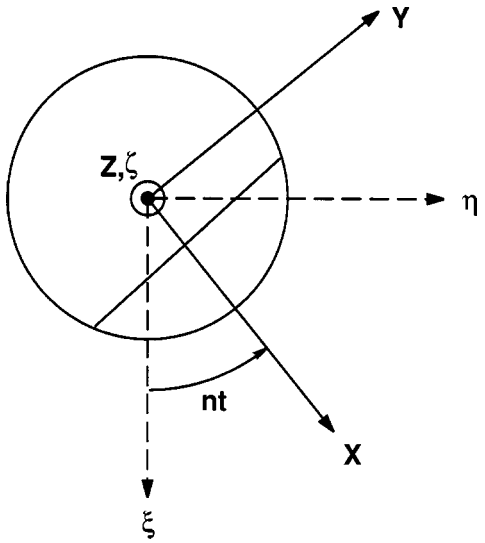


**Fig. 2 Coordinate systems**

$$\begin{bmatrix} m & 0 & 0 & 0 \\ 0 & m & 0 & 0 \\ 0 & 0 & I_t & 0 \\ 0 & 0 & 0 & I_t \end{bmatrix} \begin{Bmatrix} \ddot{X} \\ \ddot{Y} \\ \ddot{\gamma}_X \\ \ddot{\gamma}_Y \end{Bmatrix} + \begin{bmatrix} 0 & -2mn & 0 & 0 \\ 2mn & 0 & 0 & 0 \\ 0 & 0 & 0 & n(I_P-2I_t) \\ 0 & 0 & -n(I_P-2I_t) & 0 \end{bmatrix} \begin{Bmatrix} \dot{X} \\ \dot{Y} \\ \dot{\gamma}_X \\ \dot{\gamma}_Y \end{Bmatrix}$$
$$+ \begin{bmatrix} k_{11Y}-mn^2 & 0 & 0 & -k_{12Y} \\ 0 & k_{11X}-mn^2 & k_{12X} & 0 \\ 0 & k_{12X} & n^2(I_P-I_t)+k_{22X} & 0 \\ -k_{12Y} & 0 & 0 & n^2(I_P-I_t)+k_{22Y} \end{bmatrix} \begin{Bmatrix} X \\ Y \\ \gamma_X \\ \gamma_Y \end{Bmatrix} = \{F\}, \quad (1)$$

where $X$, $Y$, $\gamma_X$, and $\gamma_Y$ are displacements and tilts about the $X$ and $Y$ axes, respectively, $m$ is the mass or the rotor, $n$ is the shaft speed, $I_p$ and $I_t$ are the polar and transverse moments of inertia of the rotor, and $k_{ij}$ are stiffness elements, which are determined in the Appendix. Since in the tested system the mass of the shaft is significantly less than the mass of the rotor, it is neglected. The effects of internal energy dissipation in the free response analysis are negligible. Therefore internal damping will be incorporated into the equations of motion for the forthcoming forced response analysis. Equation (1) forms a system of coupled linear ordinary differential equations including gyroscopic effects, where $\{F\}$ is a vector of generalized applied forces.

**2.1 Undamped Free Response.** The goal of the free response analysis is to obtain the system eigenvalues, which are the natural, or whirl, frequencies. The homogeneous form of the matrix equation of motion given in Eq. (1) has the general form

$$[M]\{\ddot{S}\}+[C]\{\dot{S}\}+[K]\{S\}=\{0\}, \quad (2)$$

where $[M]$, $[C]$, and $[K]$ are inertia, "damping" (i.e., Coriolis and gyroscopic effects), and stiffness matrices, and $\{S\}$ is the generalized vector of displacements. The system is conveniently expressed in a state-variable form by defining the following $[A]$ and $[B]$ matrices:

$$[A]=\begin{bmatrix} -[K] & [0] \\ [0] & [M] \end{bmatrix}; \quad [B]=\begin{bmatrix} [0] & -[K] \\ -[K] & -[C] \end{bmatrix}. \quad (3)$$

The system expressed in state-variable form is then given by

$$\{\dot{\hat{S}}\}=[A]^{-1}[B]\{\hat{S}\}, \quad (4)$$

where $\{\hat{S}\}$ is the state vector of the displacements and tilts and their first derivatives, which is given by

$$\{\hat{S}\}=\{X \;\; Y \;\; \gamma_X \;\; \gamma_Y \;\; \dot{X} \;\; \dot{Y} \;\; \dot{\gamma}_X \;\; \dot{\gamma}_Y\}^T. \quad (5)$$

For this state vector form the state matrix is formed by $[A]^{-1}[B]$.

The eigenvalues and eigenvectors, or whirl frequencies and mode shapes, are then obtained, corresponding to the state vector expressed in the rotating $XYZ$ frame. For monitoring purposes the absolute whirl frequencies are of interest since the monitoring system is typically fixed in the inertial $\xi\eta\zeta$ coordinate frame. The absolute whirl frequencies, $\omega$, i.e., the eigenvalues expressed in the inertial $\xi\eta\zeta$ frame, can be obtained from

$$\omega=\omega_0+n, \quad (6)$$

where $\omega_0$ is the relative whirl frequency, and $n$ is the shaft speed. Since the state matrix, $[A]^{-1}[B]$, is $8\times8$, four conjugate pairs of eigenvalues are obtained. The eigenvalues are purely imaginary since damping or dissipation effects are neglected in this free response analysis.

In rotordynamics, the sign of the frequency is meaningful due to the fact that shaft whirl can occur with a negative sense, opposing the direction of shaft rotation, or a positive sense, in the direction of shaft rotation. The proper sign can be assigned to the magnitude of each eigenvalue pair which yields forward or backward whirl according to the analysis detailed in Ref. [35]. The relative whirl frequencies resulting from the analysis, $\omega_0$, are assigned the appropriate direction and the absolute whirl frequencies $\omega$ are obtained from Eq. (6). Figures 3 show the whirl frequencies as a function of shaft speed for simulated crack depths ranging from 0–40% of the shaft diameter. The "$\times$" symbols along the horizontal axis of Fig. 3 indicate shaft speeds for which one or more of the eigenvalues has a positive real part, i.e., shaft speeds for which the response is unstable. This instability is solely due to an asymmetric cross section of a purely elastic shaft (recall that internal damping has been neglected in this section) (see also Refs. [11,12,14]). Two reference lines are also plotted in each of the figures. The intersection of the $\omega=n$ line with the locus of whirl frequencies indicates shaft speeds which are equivalent to a whirl frequency, i.e., primary ($1X$) critical speeds. The intersection of the $\omega=2n$ line with the locus of whirl frequencies indicates shaft speeds which are one-half of a whirl frequency, i.e., secondary ($2X$) critical speeds.

When operating at a secondary critical speed, the $2X$ component of the response of the system is occurring at a natural frequency of the system, and will therefore exhibit a resonance behavior. It is at these $2X$ critical speeds that the $2X$ response is expected to be maximum. Comparing the predicted shaft speeds at which the $2X$ resonance occurs for various crack depths clearly shows a decrease in the natural frequencies of the system due to the presence of the crack. This change in the system natural frequency is due to the reduction in system stiffness resulting from the crack. The predicted $2X$ resonance shaft speeds for the global asymmetry crack model are given in Table 1.

**2.2 Damped Forced Response.** The gravity forced response of the system model containing the global asymmetry crack model is fundamentally important when considering crack detection. The resulting $2X$ harmonic response is the most reliable and widely used indicator of crack existence.

Energy dissipation effects are included in this analysis in order to observe the influence of the introduction and propogation of the simulated crack on the magnitude of the system response at $2X$ resonance shaft speeds. The equivalent viscous damping coefficients are incorporated into the matrix equation of motion by defining a new damping matrix, $[\hat{C}]$, according to

$$[\hat{C}]=[C]+[D], \quad (7)$$

where $[C]$ is the matrix which contains the Coriolis and gyroscopic effects, and the $[D]$ matrix contains the equivalent viscous damping coefficients. The damping matrix $[D]$ is given by

$$[D]=\begin{bmatrix} d_{11_Y} & 0 & 0 & -d_{12_Y} \\ 0 & d_{11_X} & d_{12_X} & 0 \\ 0 & d_{12_X} & d_{22_X} & 0 \\ -d_{12_Y} & 0 & 0 & d_{22_Y} \end{bmatrix}, \quad (8)$$

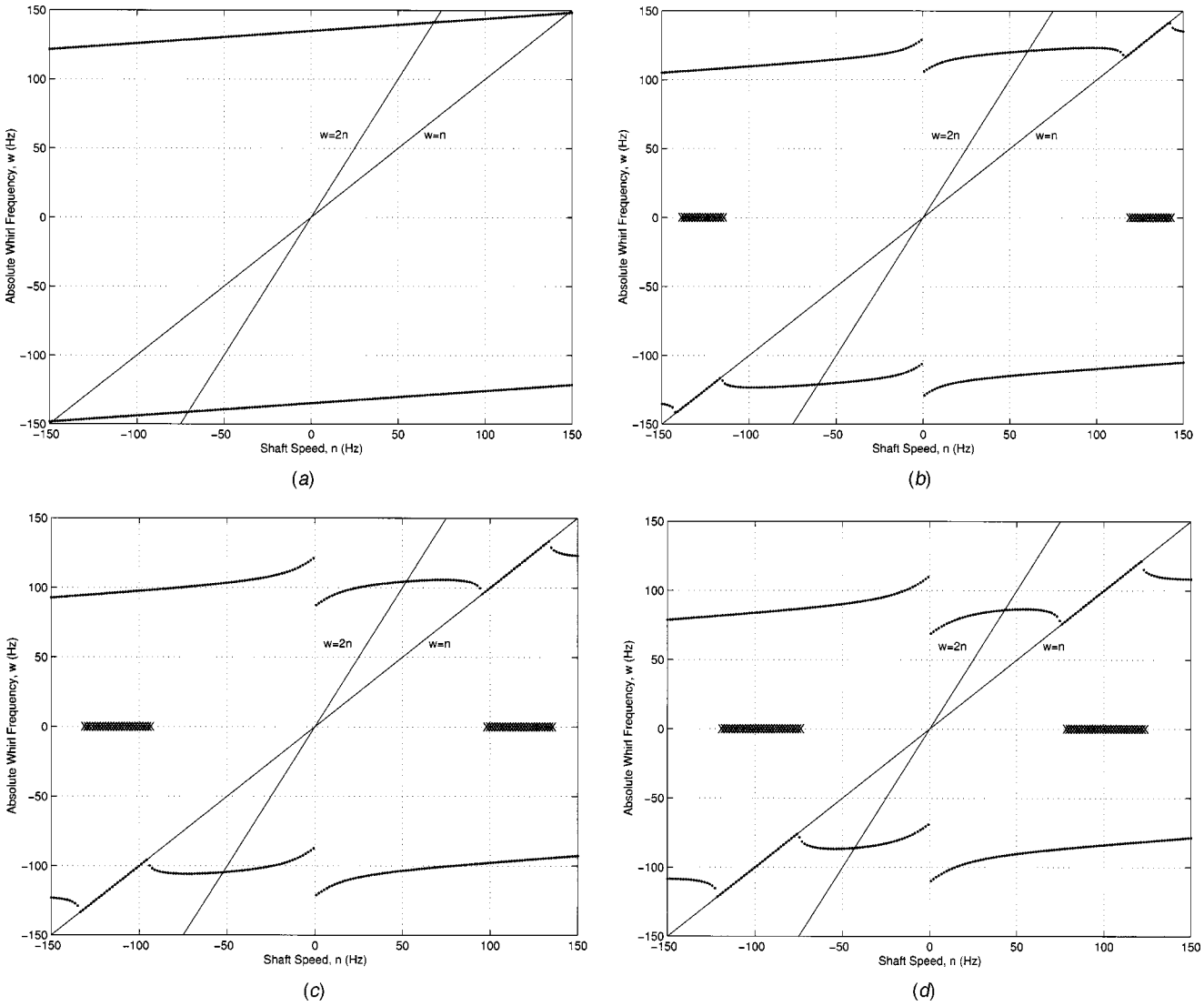


**Fig. 3 Global asymmetry model free response at various crack depth values: (*a*) uncracked; (*b*) 20%; (*c*) 30%; (*d*) 40%**

where $d_{ij_X}=d_{ij_Y}=c_{eq_{ij}}=\frac{1}{2}\overline{\beta}(k_{ij_X}+k_{ij_Y})/\omega$. Here average stiffness elements are used so that $d_{ij_X}$ and $d_{ij_Y}$ are equal. It is necessary to construct the complex equations of motion in the following analysis. The equation of motion, including internal damping, has the form

$$[M]\{\ddot{S}\}+[\hat{C}]\{\dot{S}\}+[K]\{S\}=\{F\}. \tag{9}$$

The equations of motion are derived in the shaft-fixed $XYZ$ coordinate frame. The direction along which gravity acts, which is a stationary vector along the $\xi$ axis of the inertial $\xi\eta\zeta$ coordinate frame, can be represented by a vector that is rotating with a negative sense in the $XYZ$ frame. Therefore the forcing function resulting from gravity has the form

$$F_g=mge^{-int}, \tag{10}$$

where $m$ is the mass of the rotor, $g$ is the gravitational acceleration and $n$ is the shaft speed. The vector of forces that is now included in the right-hand side of the equations of motion [Eq. (1)] is then given, in the rotating $XYZ$ coordinate frame, by

$$\{F\}=\begin{Bmatrix} mg\cos(nt) \\ -mg\sin(nt) \\ 0 \\ 0 \end{Bmatrix}. \tag{11}$$

The equations of motion are then combined by defining the following complex variables for the displacement $\rho$ and tilt $\phi$:

$$\rho=X+iY, \tag{12}$$

$$\phi=\gamma_X+i\gamma_Y. \tag{13}$$

The resulting complex equations of motion are

**Table 1 2*X* resonance shaft speeds—global asymmetry model free response**

| % cracked | Shaft speed (Hz) |
|---|---|
| 0 | 70.62 |
| 10 | 67.04 |
| 20 | 60.55 |
| 30 | 52.29 |
| 40 | 43.01 |

$$\ddot{\rho}+D_{11}\dot{\rho}+(\omega_\rho^2-n^2)\rho-\left(\frac{\Delta k_\rho}{k_\rho}\omega_\rho^2\right)\rho^*+(2n)i\dot{\rho}+D_{12_m}\dot{\phi}$$

$$+(\omega_{\rho\phi_m}^2)i\phi+\left(\frac{\Delta k_{\rho\phi}}{k_{\rho\phi}}\omega_{\rho\phi_m}^2\right)i\phi^*=ge^{-int}, \tag{14}$$

$$\ddot{\phi}+D_{22}\dot{\phi}+\left[n^2\left(\frac{I_p}{I_t}-1\right)+\omega_\phi^2\right]\phi+\left(\frac{\Delta k_\phi}{k_\phi}\omega_\phi^2\right)\phi^*-\left[n\left(\frac{I_p}{I_t}-2\right)\right]i\dot{\phi}$$

$$-D_{12_{I_t}}i\dot{\rho}-(\omega_{\rho\phi_{I_t}}^2)i\rho+\left(\frac{\Delta k_{\rho\phi}}{k_{\rho\phi}}\omega_{\rho\phi_{I_t}}^2\right)i\rho^*=0, \tag{15}$$

where the "*" denotes the complex conjugate of the variables in Eqs. (12) and (13), and

$$\omega_\rho=\frac{k_\rho}{m},\quad \omega_\phi=\frac{k_\phi}{I_t},\quad \omega_{\rho\phi_m}=\frac{k_{\rho\phi}}{m},\quad \omega_{\rho\phi_{I_t}}=\frac{k_{\rho\phi}}{I_t},$$

$$k_\rho=\tfrac{1}{2}(k_{11_X}+k_{11_Y}),$$

$$k_\phi=\tfrac{1}{2}(k_{22_X}+k_{22_Y}),\quad k_{\rho\phi}=\tfrac{1}{2}(k_{12_X}+k_{12_Y}),\quad \Delta k_\rho=k_\rho-k_{11_Y},$$

$$\Delta k_\phi=k_\phi-k_{22_Y},\quad \Delta k_{\rho\phi}=k_{\rho\phi}-k_{12_Y},\quad D_{11}=\frac{d_{11_X}}{m}=\frac{d_{11_Y}}{m},$$

$$D_{12_m}=\frac{d_{12_X}}{m}=\frac{d_{12_Y}}{m},\quad D_{12_{I_t}}=\frac{d_{12_X}}{I_t}=\frac{d_{12_Y}}{I_t},$$

$$D_{22}=\frac{d_{22_X}}{I_t}=\frac{d_{22_Y}}{I_t}.$$

To solve this system of equations, solutions of the following forms are chosen for the displacement $\rho$, and tilt $\phi$:

$$\rho=Ae^{int}+Be^{-int}, \tag{16}$$

$$\phi=Ce^{int}+De^{-int}, \tag{17}$$

where $A$, $B$, $C$, and $D$ are arbitrary complex numbers. These solutions are substituted into Eqs. (14) and (15) and the complex coefficients $A$, $B$, $C$, and $D$ are determined. Recalling that the displacement and tilt in the rotating $XYZ$ coordinate frame are given by Eqs. (16) and (17), the displacement $u$ and tilt $\gamma$ in the inertial coordinate frame are obtained according to

$$u=\rho e^{int}, \tag{18}$$

$$\gamma=\phi e^{int}. \tag{19}$$

The displacement and tilt expressed in the inertial coordinate frame are of interest since the experimental data provided by the monitoring system is also obtained in the inertial coordinate frame (according to Ref. [35]). From Eqs. (16)–(19) it is clear that the displacement and tilt in the inertial coordinate frame will have the form

$$u=Ae^{i2nt}+B, \tag{20}$$

$$\gamma=Ce^{i2nt}+D. \tag{21}$$

The presence of the $2X$ harmonic is evident in Eqs. (20) and (21). The magnitudes of coefficients $A$ and $C$ are the magnitudes of the $2X$ harmonic response, in the inertial frame, of the displacement and tilt, respectively. Equations (20) and (21) predict displacement and tilt responses which have circular shapes, having radii of $|A|$, and $|C|$, and are offset by $B$ and $D$. It is important to note that due to the form of the assumed solutions [Eqs. (16) and (17)], the resulting solutions [Eqs. (20) and (21)] are limited to predicting only circular orbit shapes of the $2X$ component.

Figures 4 show the predicted magnitude of the $2X$ tilt response, based on the global asymmetry crack model, as a function of shaft speed, for two speed ranges, and crack depths varying from 0 to 40% of the shaft diameter. The magnitudes plotted show the radii

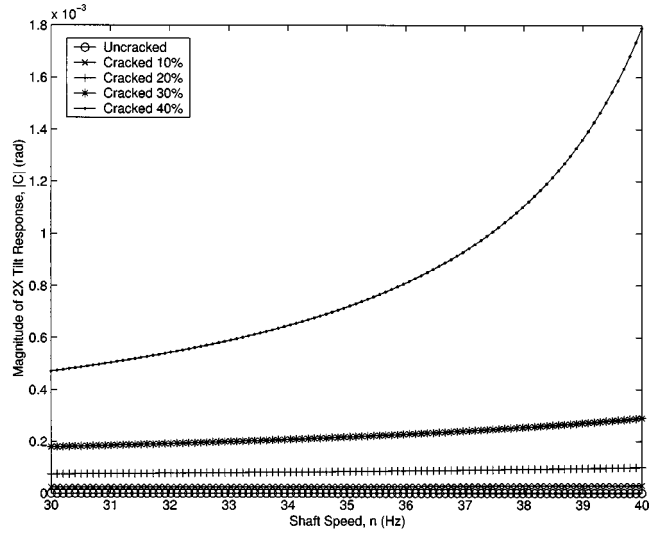


(*a*)

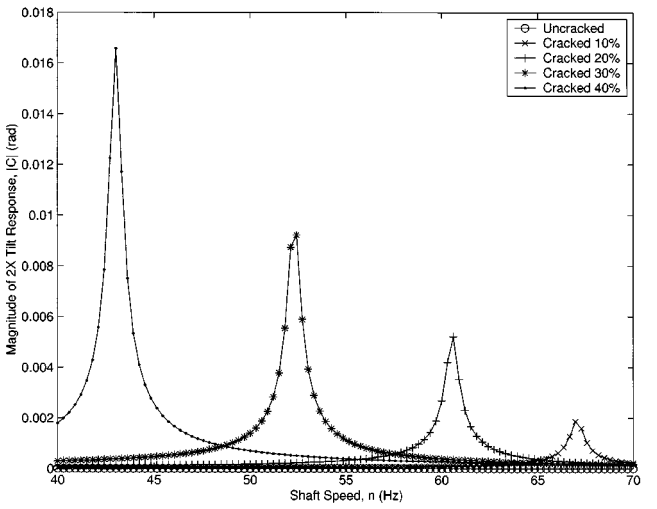


(*b*)

**Fig. 4 Global asymmetry model forced tilt $2X$ response: (*a*) Low-speed range; (*b*) high-speed range**

of the predicted circular $2X$ tilt responses. It is clear that for an arbitrary shaft speed, the amplitude of the $2X$ response is predicted to increase as the crack depth increases.

The magnitudes of the $2X$ component of the response plotted in Fig. 4(*a*) are significantly smaller than those plotted in Fig. 4(*b*). The range of shaft speeds shown in Fig. 4(*b*) contains $2X$ resonant speeds for each crack depth.

As predicted, the $2X$ resonant speeds decrease as the crack depth increases. The $2X$ resonance shaft speeds predicted based on this global asymmetry crack model forced response analysis are given in Table 2. These predicted $2X$ resonance shaft speeds agree with the $2X$ resonance shaft speeds predicted in the global asymmetry model free response analysis, which are given in Table 1. Since the 0% simulated crack depth results in a system with symmetric stiffness properties, no $2X$ resonance is predicted for the forced response analysis. Damping is light, thus numerically Tables 1 and 2 provide similar $2X$ results.

## 3 Local Asymmetry Crack Model

Perhaps the most important effect of the presence of a transverse crack in a rotating shaft is the highly localized flexibility

**Table 2 2X resonance shaft speeds—global asymmetry model forced response**

| % cracked | Shaft speed (Hz) |
|---|---|
| 0 | |
| 10 | 67.04 |
| 20 | 60.55 |
| 30 | 52.29 |
| 40 | 43.01 |

that is introduced. To locally represent the stiffness properties of a cracked cross section in an otherwise uncracked shaft, it is necessary to determine the additional flexibility due to the presence of the crack, and incorporate this flexibility into a discrete representation of the system. In this study a transfer-matrix method was employed to accomplish this desired localizing effect. Figure 5 shows the cracked system represented by three lumped stiffness elements; $[F_1]$, $[F_{\text{crack}}]$, and $[F_2]$, and one lumped inertia element $[P]$. Since the mass of the shaft is significantly less than the mass of the rotor, the mass of the shaft is neglected.

The purpose of this section is to present the analytical portion of the analysis of the cracked system including a local asymmetry crack model using the complex extended transfer-matrix method [2,37] for free and forced response analyses, along with relevant results. As previously, damping effects will be incorporated into the forced response analysis.

**3.1 Crack Flexibility.** The localized additional flexibility can be represented by a lumped parameter element. A section of a shaft containing a crack of depth $a$ is shown, under general loading, in Fig. 6($a$). Figure 6($b$) shows the cross section of the shaft section in Fig. 6($a$) at the location of the transverse crack. The generalized displacement $u_i$ in the $i$ direction is obtained by utilizing Castigliano's theorem [21,30]:

$$u_i = \frac{\partial}{\partial P_i} \int_0^{\alpha} J(Y)\, dY, \tag{22}$$

where $P_i$ is the generalized force associated with $u_i$, and $J(Y)$, according to Tada, Paris, and Irwin [37], is the strain energy density function given by

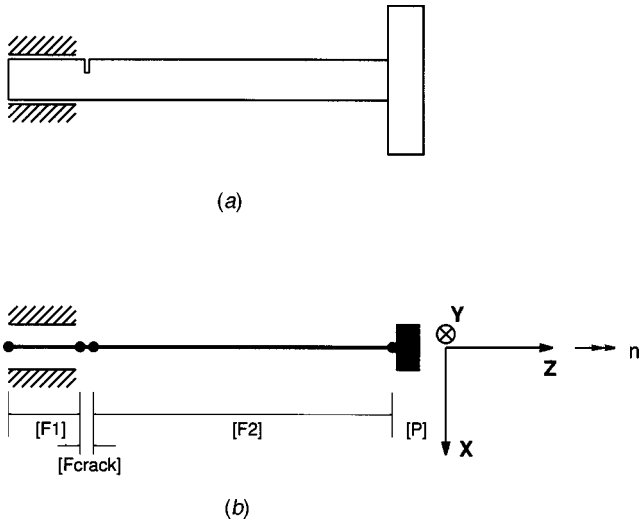


**Fig. 5 Local asymmetry crack model**

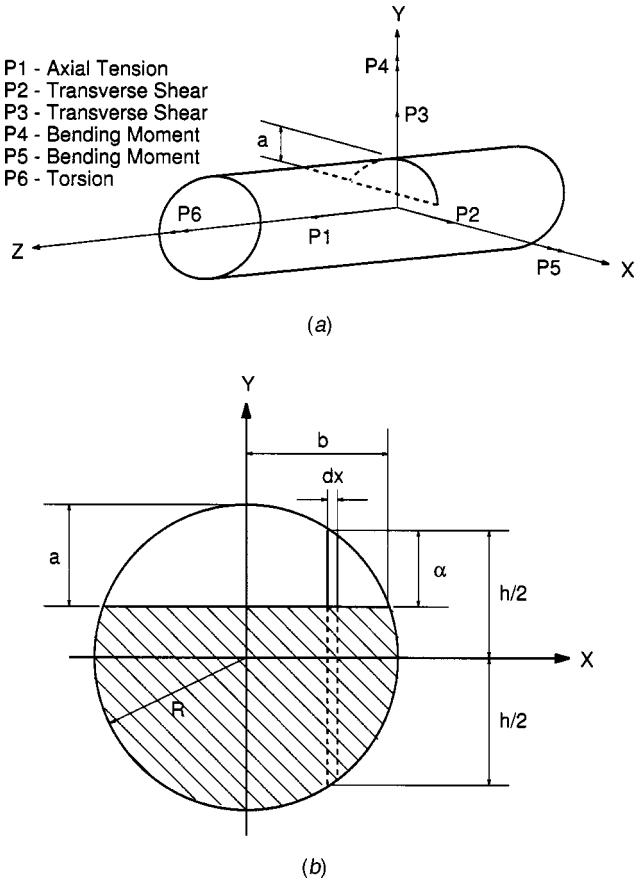


**Fig. 6 Local crack model: (*a*) shaft section containing a crack; (*b*) crack cross section**

$$J(\alpha) = \frac{1-\nu^2}{E}\left[\left(\sum_{i=1}^{6} K_{Ii}\right)^2 + \left(\sum_{i=1}^{6} K_{IIi}\right)^2 + (1+\nu)\left(\sum_{i=1}^{6} K_{IIIi}\right)^2\right], \tag{23}$$

where $\nu$ is Poisson's ratio, $E$ is Young's Modulus, and $K_{ni}$ is the crack stress intensity factor for mode $n$ due to $P_i$. The stress intensity factors for a unit width strip containing a crack of depth $\alpha$ are evaluated according to

$$K_{ni} = \sigma_i \sqrt{\pi \alpha} F_n\left(\frac{\alpha}{h}\right), \tag{24}$$

where $\sigma_i$ are the stresses due to the load $P_i$ at the crack, $F_n(\alpha/h)$ are appropriate intensity functions, and $h$ is the total strip length (see Fig. 6($b$)).

The additional flexibility due to the crack for a unit width strip can be written as

$$c_{ij} = \frac{\partial^2}{\partial P_i \partial P_j} \int_0^{\alpha} J(Y)\, dY \tag{25}$$

which, after integration along the crack edge, becomes

$$c_{ij} = \frac{\partial^2}{\partial P_i \partial P_j} \int_{-b}^{b} \int_0^{\alpha} J(Y)\, dY. \tag{26}$$

The current analysis is not concerned with torsion or axial displacement, hence only $c_{22}$, $c_{33}$, $c_{44}$, $c_{45}$, $c_{54}$, and $c_{55}$ are required. These elements are then given by

$$c_{22}=\frac{4(1-\nu^2)}{\pi ER}\int_0^{\bar{b}}\int_0^{\bar{a}}\bar{Y}F_{II}^2\left(\frac{\bar{Y}}{\bar{h}}\right)d\bar{Y}d\bar{X}, \tag{27}$$

$$c_{33}=\frac{4(1-\nu^2)}{\pi ER}\int_0^{\bar{b}}\int_0^{\bar{a}}\bar{Y}F_{II}^2\left(\frac{\bar{Y}}{\bar{h}}\right)d\bar{Y}d\bar{X}, \tag{28}$$

$$c_{44}=\frac{32(1-\nu^2)}{\pi ER^3}\int_0^{\bar{b}}\int_0^{\bar{a}}\bar{X}^2\bar{Y}F_{IY}^2\left(\frac{\bar{Y}}{\bar{h}}\right)d\bar{Y}d\bar{X}, \tag{29}$$

$$c_{45}=c_{55}=\frac{64(1-\nu^2)}{\pi ER^3}\int_0^{\bar{b}}\int_0^{\bar{a}}\bar{X}\bar{Y}\sqrt{1-\bar{X}^2}F_{IX}\left(\frac{\bar{Y}}{\bar{h}}\right)F_{IY}\left(\frac{\bar{Y}}{\bar{h}}\right)d\bar{Y}d\bar{X}, \tag{30}$$

$$c_{55}=\frac{64(1-\nu^2)}{\pi ER^3}\int_0^{\bar{b}}\int_0^{\bar{a}}(1-\bar{X}^2)\bar{Y}F_{IX}^2\left(\frac{\bar{Y}}{\bar{h}}\right)d\bar{Y}d\bar{X}, \tag{31}$$

where $\bar{b}=b/R$, $\bar{X}=X/R$, $\bar{Y}=Y/R$, $\bar{\alpha}=\alpha/R$, and $\bar{h}=h/R$. The corresponding intensity functions are given by

$$F_{IX}\left(\frac{\alpha}{h}\right)=\left[\frac{\tan(\beta_c)}{\beta_c}\right]^{1/2}[.932+.199(1-\sin(\beta_c))^4]/\cos(\beta_c), \tag{32}$$

$$F_{IY}\left(\frac{\alpha}{h}\right)=\left[\frac{\tan(\beta_c)}{\beta_c}\right]^{1/2}\left[.752+.202\left(\frac{\alpha}{h}\right)+.37(1-\sin(\beta_c))^3\right]\Big/\cos(\beta_c), \tag{33}$$

$$F_{II}\left(\frac{\alpha}{h}\right)=\left[1.122-.561\left(\frac{\alpha}{h}\right)+.085\left(\frac{\alpha}{h}\right)^2+.18\left(\frac{\alpha}{h}\right)^3\right]\Big/\left(1-\frac{\alpha}{h}\right)^{1/2}, \tag{34}$$

$$F_{III}\left(\frac{\alpha}{h}\right)=\left[\frac{\tan(\beta_c)}{\beta_c}\right]^{1/2}, \tag{35}$$

$$\beta_c=\left(\frac{\pi\alpha}{2h}\right). \tag{36}$$

The additional flexibilities due to the presence of the crack may therefore be obtained by numerically integrating Eqs. (27)–(31). Dimensionless flexibilities can be obtained according to

$$\bar{c}_{22}=c_{22}\frac{\pi ER}{(1-\nu^2)},\quad \bar{c}_{33}=c_{33}\frac{\pi ER}{(1-\nu^2)},$$
$$\bar{c}_{44}=c_{44}\frac{\pi ER^3}{(1-\nu^2)}\quad \bar{c}_{45}=c_{45}\frac{\pi ER^3}{(1-\nu^2)}, \tag{37}$$
$$\bar{c}_{55}=c_{55}\frac{\pi ER^3}{(1-\nu^2)},$$

where the overbar indicates the nondimensional value. These dimensionless flexibilities are plotted in Fig. 7, for crack depths up to 50% of the shaft diameter. These local flexibilities may now be introduced appropriately into the discrete representation of the system.

**3.2 Transfer Matrix.** The transfer-matrix method is a lumped parameter method in which inertial properties of the system are lumped into point matrices, and stiffness properties of the system are represented by lumped field matrices [2]; both relate state vectors at the two ends of a shaft element. The state vector at station *i*, expressed in the rotating *XYZ* coordinate frame, is defined as

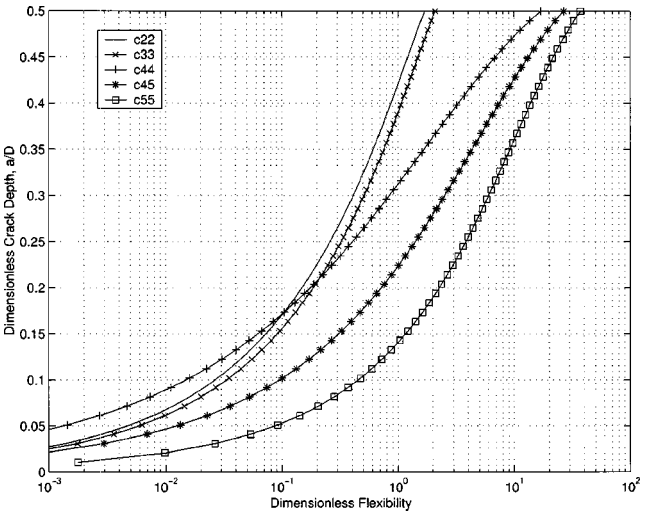


**Fig. 7 Dimensionless crack flexibilities**

$$\{Z\}_i=\{u_X\ \ \theta_Y\ \ M_Y\ \ -V_X\ \ -u_Y\ \ \theta_X\ \ M_X\ \ V_Y\}^T, \tag{38}$$

where $u$, $\theta$, $M$, and $V$ are the complex magnitudes of the displacement, tilt, moment, and shear force, respectively.

*The Field Matrix.* The state vector at the left of station *i*, $\{Z\}_i^L$, is related to the state vector at the right of station $i-1$, $\{Z\}_{i-1}^R$, by the field matrix $[F_i]$:

$$\{Z\}_i^L=[F_i]\{Z\}_{i-1}^R. \tag{39}$$

The field matrix $[F_i]$ has the form

$$[F_i]=\begin{bmatrix} 1 & l_i & \frac{l_i^2}{2EI} & \frac{l_i^3}{6EI} & 0 & 0 & 0 & 0\\ 0 & 1 & \frac{l_i}{EI} & \frac{l_i^2}{2EI} & 0 & 0 & 0 & 0\\ 0 & 0 & 1 & l_i & 0 & 0 & 0 & 0\\ 0 & 0 & 0 & 1 & 0 & 0 & 0 & 0\\ 0 & 0 & 0 & 0 & 1 & l_i & \frac{l_i^2}{2EI} & \frac{l_i^3}{6EI}\\ 0 & 0 & 0 & 0 & 0 & 1 & \frac{l_i}{EI} & \frac{l_i^2}{2EI}\\ 0 & 0 & 0 & 0 & 0 & 0 & 1 & l_i\\ 0 & 0 & 0 & 0 & 0 & 0 & 0 & 1 \end{bmatrix}, \tag{40}$$

where $l_i$ is the length of the field, $E$ is Young's modulus, and $I$ is the area moment of inertia of the field cross section.

*The Crack Matrix.* The crack is represented by a field matrix which contains the additional flexibilities introduced by the presence of the crack. The crack field matrix $[F_{\text{crack}}]$ has the form

$$[F_{crack}]=\begin{bmatrix} 1 & 0 & 0 & -c_{22} & 0 & 0 & 0 & 0 \\ 0 & 1 & c_{44} & 0 & 0 & 0 & c_{45} & 0 \\ 0 & 0 & 1 & 0 & 0 & 0 & 0 & 0 \\ 0 & 0 & 0 & 1 & 0 & 0 & 0 & 0 \\ 0 & 0 & 0 & 0 & 1 & 0 & 0 & -c_{33} \\ 0 & 0 & c_{54} & 0 & 0 & 1 & c_{55} & 0 \\ 0 & 0 & 0 & 0 & 0 & 0 & 1 & 0 \\ 0 & 0 & 0 & 0 & 0 & 0 & 0 & 1 \end{bmatrix}, \tag{41}$$

where the elements $c_{ij}$ are determined in Eqs. (27)–(36). Notably, in an uncracked shaft, $a=0$, $c_{ij}=0$, and $[F_{\text{crack}}]=[I]$.

*The Point Matrix.* The state vector at the right of the lumped mass at station $i$, $\{Z\}_i^R$, is related to the state vector at the left of the lumped mass at station $i$, $\{Z\}_i^L$, by the point matrix $[P_i]$:

$$\{Z\}_i^R=[P_i]\{Z\}_i^L. \tag{42}$$

The solution is sought in the rotating frame, $XYZ$, thus

$$[P_i]=\begin{bmatrix} 1 & 0 & 0 & 0 & 0 & 0 & 0 & 0 \\ 0 & 1 & 0 & 0 & 0 & 0 & 0 & 0 \\ 0 & n^2(I_p-I_t)-I_t\omega_0^2 & 1 & 0 & 0 & in\omega_0(2I_t-I_p) & 0 & 0 \\ m(\omega_0^2+n^2) & 0 & 0 & 1 & -2in\omega_0 m & 0 & 0 & 0 \\ 0 & 0 & 0 & 0 & 1 & 0 & 0 & 0 \\ 0 & 0 & 0 & 0 & 0 & 1 & 0 & 0 \\ 0 & in\omega_0(2I_t-I_p) & 0 & 0 & 0 & n^2(I_p-I_t)-I_t\omega_0^2 & 1 & 0 \\ 2in\omega_0 m & 0 & 0 & 0 & m(\omega_0^2+n^2) & 0 & 0 & 1 \end{bmatrix}, \tag{43}$$

where $m$ is the rotor mass, $I_t$ and $I_p$ are the transverse and polar mass moments of inertia, respectively, $n$ is the shaft speed, and $\omega_0$ is the relative whirl frequency (see Eqs. (1) and (6)).

*The Overall Transfer Matrix.* The overall transfer matrix for this system, $[U]$, is constructed according to

$$[U]=[P][F_2][F_{\text{crack}}][F_1]. \tag{44}$$

The state at the support, $\{Z\}_{\text{support}}$, is then related to the state at the right of the lumped mass $\{Z\}_1^R$ by the following:

$$\{Z\}_1^R=[U]\{Z\}_{\text{support}}. \tag{45}$$

*Undamped Free Response.* Applying the clamped-free boundary conditions, which are no displacement or tilt at the support boundary and no shear or moment at the end of the shaft, to the overall transfer matrix expression given in Eq. (45) leads to the following relations:

$$\begin{bmatrix} U_{33} & U_{34} & U_{37} & U_{38} \\ U_{43} & U_{44} & U_{47} & U_{48} \\ U_{73} & U_{74} & U_{77} & U_{78} \\ U_{83} & U_{84} & U_{87} & U_{88} \end{bmatrix} \begin{Bmatrix} M_Y \\ -V_X \\ M_X \\ V_Y \end{Bmatrix}_{\text{support}} \triangleq [\text{Freq}] \begin{Bmatrix} M_Y \\ -V_X \\ M_X \\ V_Y \end{Bmatrix}_{\text{support}} = \begin{Bmatrix} 0 \\ 0 \\ 0 \\ 0 \end{Bmatrix}_1^R, \tag{46}$$

$$\begin{bmatrix} U_{13} & U_{14} & U_{17} & U_{18} \\ U_{23} & U_{24} & U_{27} & U_{28} \\ U_{53} & U_{54} & U_{57} & U_{58} \\ U_{63} & U_{64} & U_{67} & U_{68} \end{bmatrix} \begin{Bmatrix} M_Y \\ -V_X \\ M_X \\ V_Y \end{Bmatrix}_{\text{support}} \triangleq [\text{Switch}] \begin{Bmatrix} M_Y \\ -V_X \\ M_X \\ V_Y \end{Bmatrix}_{\text{support}} = \begin{Bmatrix} u_X \\ \theta_Y \\ -u_Y \\ \theta_X \end{Bmatrix}_1^R, \tag{47}$$

where $U_{ij}$ are elements of the overall transfer matrix $[U]$.

By solving the standard eigenvalue problem for Eq. (46), four complex-conjugate pairs of eigenvalues result. The problem of assigning whirl directions to each of the four frequency magnitudes is identical to the previous discussion. To obtain the mode shape for a given eigenvalue, which is essentially the displacement and tilt portion of the state vector at the end of the shaft, it is convenient to label the 4×4 matrices in Eqs. (46) and (47) as [Freq] and [Switch], respectively. From Eq. (47), the shear and moment portion of the state vector at the support is given by

$$\begin{Bmatrix} M_Y \\ -V_X \\ M_X \\ V_Y \end{Bmatrix}_{\text{support}} = [\text{Switch}]^{-1} \begin{Bmatrix} u_X \\ \theta_Y \\ -u_Y \\ \theta_X \end{Bmatrix}_1^R. \tag{48}$$

Substituting this expression for $\{M_Y\ -V_X\ M_X\ V_Y\}_{\text{support}}^T$ into Eq. (46) results in

$$[\text{Freq}][\text{Switch}]^{-1} \begin{Bmatrix} u_X \\ \theta_Y \\ -u_Y \\ \theta_X \end{Bmatrix}_1^R = \begin{Bmatrix} 0 \\ 0 \\ 0 \\ 0 \end{Bmatrix}. \tag{49}$$

For each frequency magnitude, given by the four pairs of eigenvalues, Eq. (49) forms a linearly dependent system of equations. Solving this eigenvalue problem results in the corresponding mode shape, i.e., the vector $\{u_X\ \theta_Y\ u_Y\ \theta_X\}^T$. Once the eigenvalues and corresponding eigenvectors, or mode shapes, are determined, whirl directions are also assigned (see previous discussion) to each frequency, and the true natural frequencies are plotted versus shaft speed.

Figure 8 shows the whirl frequencies as a function of shaft speed for crack depths ranging from 0 to 40% of the shaft diameter. The "×" symbols along the horizontal axis indicate shaft speeds for which one or more of the eigenvalues has a positive real part, i.e., shaft speeds for which the response is unstable. As previously, two reference lines indicating critical speeds and "2$X$ resonance" shaft speeds are also included in each figure. From

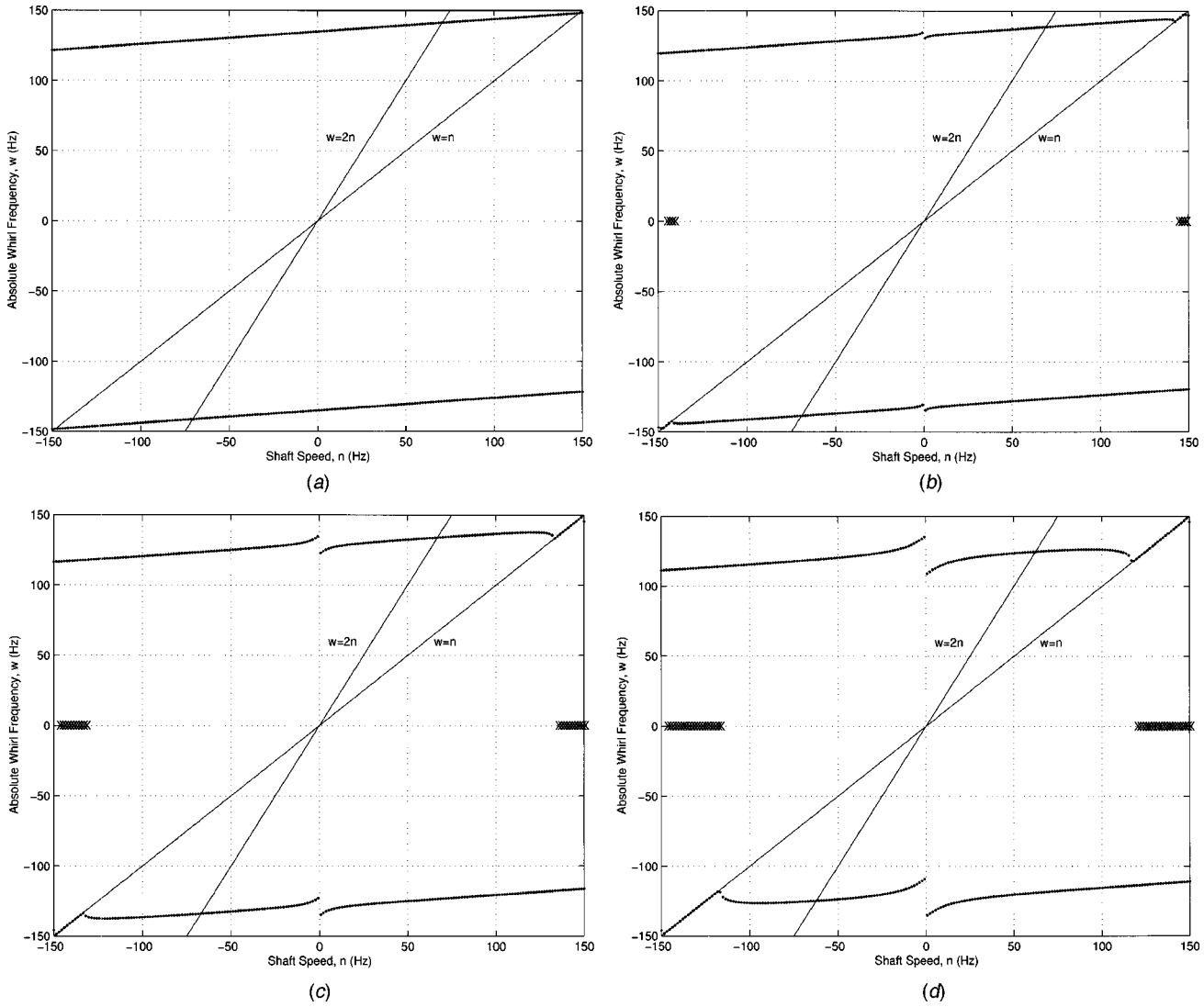


**Fig. 8 Local asymmetry model free response at various crack values: (*a*) uncracked; (*b*) 20%; (*c*) 30%; (*d*) 40%**

this analysis, shaft speeds at which the $2X$ response is maximum can be predicted for various crack depths. Table 3 gives the predicted $2X$ resonance shaft speeds based on the local asymmetry crack model. The decrease in the $2X$ resonance shaft speeds indicates the decrease in the natural frequencies of the system resulting from the increased flexibility introduced by the presence of the crack. This free response analysis of the system containing the local asymmetry crack model indicates that a decrease in natural frequencies, which may be observed as a decrease in primary and secondary critical speeds, is a characteristic of the system response that can be directly attributed to the presence of a transverse crack.

**Table 3 $2X$ resonance shaft speeds—local asymmetry model free response**

| % cracked | Shaft speed (Hz) |
|---|---|
| 0 | 70.62 |
| 10 | 70.34 |
| 20 | 69.24 |
| 30 | 66.97 |
| 40 | 62.44 |

*Damped Forced Response.* To account for a forcing function in the transfer-matrix method described above, the state vector and field and point matrices are extended to $9\times1$ and $9\times9$, respectively, similar to Ref. [2]. Likewise, the point matrix for this local asymmetry model forced response analysis will be modified to include damping effects.

The state vector for station $i$ now has the form

$$\{Z\}_i=\{u_X\ \ \theta_Y\ \ M_Y\ \ -V_X\ \ -u_Y\ \ \theta_X\ \ M_X\ \ V_Y\ \ 1\}^T. \quad (50)$$

The field matrices, including the crack matrix, are identical to those given in Eqs. (40) and (41) with an additional row and column of zeros, except for element (9,9), which is one unit. The damped forced response point matrix $[\hat{P}_i]$ contains damping effects, and is given by

$$[\hat{P}_i]=\begin{bmatrix}[P_i] & \{0\}\\ \{0\} & 1\end{bmatrix}+[\tilde{P}_i], \quad (51)$$

where $[P_i]$ is the $8\times8$ point matrix given in Eq. (43), and $[\tilde{P}_i]$ is the $9\times9$ matrix given by

$$[\tilde{P}_i]=\begin{bmatrix} 0 & 0 & 0 & 0 & 0 & 0 & 0 & 0 & 0 \\ 0 & 0 & 0 & 0 & 0 & 0 & 0 & 0 & 0 \\ i\omega d_{12_Y} & -i\omega d_{22_Y} & 0 & 0 & 0 & 0 & 0 & 0 & 0 \\ i\omega d_{11_Y} & -i\omega d_{12_Y} & 0 & 0 & 0 & 0 & 0 & 0 & mg \\ 0 & 0 & 0 & 0 & 0 & 0 & 0 & 0 & 0 \\ 0 & 0 & 0 & 0 & 0 & 0 & 0 & 0 & 0 \\ 0 & 0 & 0 & 0 & i\omega d_{12_X} & -i\omega d_{22_X} & 0 & 0 & 0 \\ 0 & 0 & 0 & 0 & i\omega d_{11_X} & -i\omega d_{12_X} & 0 & 0 & -img \\ 0 & 0 & 0 & 0 & 0 & 0 & 0 & 0 & 0 \end{bmatrix}, \tag{52}$$

where $d_{ij_q}=c_{eq_{ij_q}}=\overline{\beta}k_{ij_q}/\omega$, and $g$ is the acceleration due to gravity. This matrix contains the influence of internal damping and the forcing function. The overall transfer matrix is obtained by combining these $9\times9$ field and point matrices as in Eqs. (44) and (45). Applying the clamped-free boundary conditions, which are no displacement or tilt at the support boundary and no shear or moment at the end of the shaft, results in the following relations for the forced response:

$$\begin{bmatrix} U_{33} & U_{34} & U_{37} & U_{38} \\ U_{43} & U_{44} & U_{47} & U_{48} \\ U_{73} & U_{74} & U_{77} & U_{78} \\ U_{83} & U_{84} & U_{87} & U_{88} \end{bmatrix} \begin{Bmatrix} M_Y \\ -V_X \\ M_X \\ V_Y \end{Bmatrix}_{\text{support}} + \begin{Bmatrix} U_{39} \\ U_{49} \\ U_{79} \\ U_{89} \end{Bmatrix} = \begin{Bmatrix} 0 \\ 0 \\ 0 \\ 0 \end{Bmatrix}_1^R, \tag{53}$$

$$\begin{bmatrix} U_{13} & U_{14} & U_{17} & U_{18} \\ U_{23} & U_{24} & U_{27} & U_{28} \\ U_{53} & U_{54} & U_{57} & U_{58} \\ U_{63} & U_{64} & U_{67} & U_{68} \end{bmatrix} \begin{Bmatrix} M_Y \\ -V_X \\ M_X \\ V_Y \end{Bmatrix}_{\text{support}} = \begin{Bmatrix} u_X \\ \theta_Y \\ -u_Y \\ \theta_X \end{Bmatrix}_1^R. \tag{54}$$

The vector $\{M_Y\ -V_X\ M_X\ V_Y\}^T$ in Eq. (53) is obtained as the solution of a linearly independent system of equations. This solution is substituted into Eq. (54) and the forced response vector $\{u_X\ \theta_Y\ u_Y\ \theta_X\}^T$ is obtained. Each element of the state vector is a complex number. The displacement in the $X$ and $Y$ directions, for example, are of the form

$$u_X=u_{X_r}+iu_{X_i}, \tag{55}$$

$$u_Y=u_{Y_r}+iu_{Y_i}, \tag{56}$$

where the $r$ and $i$ subscripts denote real and imaginary components, respectively. The displacement in the $X$ and $Y$ directions, $X$ and $Y$, will be given by

$$X=\text{Re}[u_Xe^{int}], \tag{57}$$

$$Y=\text{Re}[u_Ye^{int}]. \tag{58}$$

So, taking the real part of each,

$$X=u_{X_r}\cos(nt)-u_{X_i}\sin(nt), \tag{59}$$

$$Y=u_{Y_r}\cos(nt)-u_{Y_i}\sin(nt). \tag{60}$$

Recalling that the point and field matrices were derived in the rotating coordinate frame $XYZ$,

$$\rho=X+iY=(u_{X_r}+iu_{Y_r})\cos(nt)-(u_{X_i}+iu_{Y_i})\sin(nt). \tag{61}$$

It is desired to observe the results in a stationary coordinate frame. The transformation from the rotating $XYZ$ coordinate frame to the inertial $\xi\eta\zeta$ coordinate frame is given by

$$u=\rho e^{int}, \tag{62}$$

so, the displacement of the rotor expressed in the stationary coordinate frame is

$$u=\tfrac{1}{2}[(u_{X_r}-iu_{x_i}+iu_{Y_r}+u_{Y_i})+(u_{X_r}+iu_{x_i}+iu_{Y_r}-u_{Y_i})e^{i2nt}]. \tag{63}$$

Similarly, the tilt of the rotor expressed in the stationary coordinate frame is

$$\gamma=\tfrac{1}{2}[(\theta_{X_r}-i\theta_{x_i}+i\theta_{Y_r}+\theta_{Y_i})+(\theta_{X_r}+i\theta_{x_i}+i\theta_{Y_r}-\theta_{Y_i})e^{i2nt}]. \tag{64}$$

It is clear from Eqs. (63) and (64) that the constant radial force of gravity acting on the cracked system results in a $2X$ harmonic response which is predicted by this analysis to have a circular shape. The predicted $2X$ circular tilt response has a radius of $\frac{1}{2}|(\theta_{X_r}-\theta_{Y_i})+i(\theta_{X_i}+\theta_{Y_r})|$ and is offset according to $\frac{1}{2}[(\theta_{X_r}+\theta_{Y_i})-i(\theta_{X_i}-\theta_{Y_r})]$. The magnitude of the $2X$ tilt response is plotted as a function of shaft speed in Fig. 9, shown separately for two low- and high-speed ranges, and for crack depths varying from 0 to 40% of the shaft diameter. It is clear that for an arbitrary shaft speed, the amplitude of the $2X$ response is predicted to increase as the crack depth increases. The range of shaft speeds shown contains $2X$ resonant speeds for each crack depth (Fig. 9(*b*)). As previously, the $2X$ resonant speeds decrease as the crack depth increases. The $2X$ resonance shaft speeds predicted based on this local asymmetry crack model forced response analysis are given in Table 4. Since the 0% crack depth results in a system with symmetric stiffness properties, no $2X$ resonance is predicted for the forced response analysis. Damping is light (typical damping ratios are less than 1%, as experimentally found [35]), thus numerically Tables 3 and 4 provide similar $2X$ results.

The amplitude of the $2X$ response at each $2X$ resonant speed is shown to increase in magnitude as the crack depth increases. The shaft speeds at which the $2X$ peaks occur decrease due to the reduced stiffness, which changes the system natural frequencies, resulting from the presence of the crack. The increased amplitude of the $2X$ component of the system response is due to the increased asymmetry as the crack depth increases. This forced response analysis of the system containing the local asymmetry crack model indicates that an increase in the amplitude of the $2X$ component of the system response, as well as a decrease in the shaft speed at which the $2X$ component of the response is maximum, are characteristics of the system response that may be directly attributed to the presence of a transverse shaft crack.

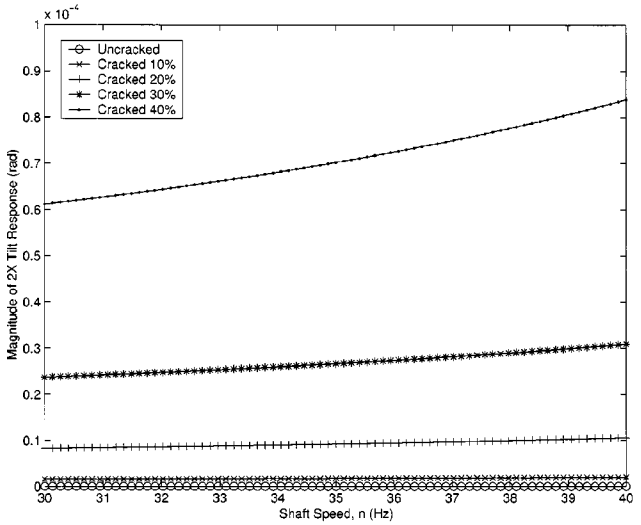


(*a*)

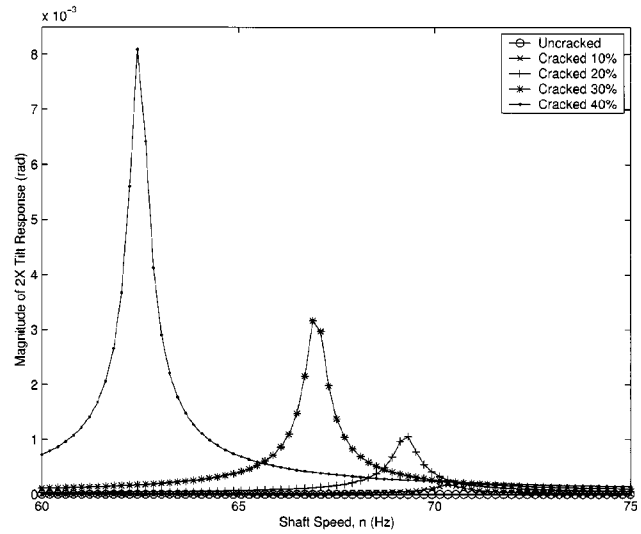


(*b*)

**Fig. 9 Local asymmetry model forced response: (*a*) low-speed range; (*b*) high-speed range**

## 4 Conclusions

Two theoretical analyses have been presented to identify characteristics of the system response that may be directly attributed to the presence of a transverse crack in the shaft of the test rig system. Both the global and local asymmetry crack model analyses qualitatively predict response characteristics which have been experimentally observed in the response of a system containing a gaping crack.

The behavior of the $2X$ harmonic component of the system response is an effective target observation for a monitoring system. The predicted behaviors of the $2X$ harmonic component of the system response include an increase in magnitude for increasing crack depth as well as a decrease in the shaft speed at which the $2X$ harmonic component of the system response is maximum. The presence of a transverse shaft crack has also been shown to induce an unstable response for some shaft speeds. The detection of changes in the magnitude of the $2X$ harmonic component of the system response becomes much more difficult for shaft speeds which are greater than $2X$ resonance speeds. Frequency-sweep tests, which pass through $2X$ resonance shaft speeds, would provide the most useful information; however, observation of the magnitude of the $2X$ component could also provide crack diagnostic information.

This research utilizes a method to account for a shaft crack in the transfer-matrix method. By employing these transfer matrices, coupled systems that include shafts, seals, bearings, etc., can be systematically analyzed in a modular fashion [2].

**Table 4 $2X$ resonance shaft speeds—local asymmetry model forced response**

| % cracked | Shaft speed (Hz) |
|---|---|
| 0 | |
| 10 | 70.34 |
| 20 | 69.24 |
| 30 | 66.97 |
| 40 | 62.44 |

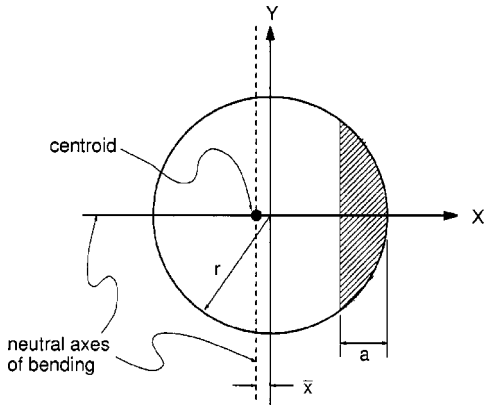


**Fig. 10 Asymmetric shaft cross section**

## Acknowledgments

This research was conducted under Grant No. N00014-95-1-0539 of the Office of Naval Research. Dr. Peter Schmidt was the Program Manger. This support is gratefully acknowledged.

## Appendix: Asymmetric Stiffness

The stiffness elements relate the displacement and tilt at the end of the shaft to the applied forces or moments in the $X$ and $Y$ directions. The stiffness relationships for a cantilever Euler-Bernoulli beam are obtained from general beam theory as

$$\begin{Bmatrix} F_X \\ M_Y \end{Bmatrix} = \begin{bmatrix} k_{11_Y} & -k_{12_Y} \\ -k_{21_Y} & k_{22_Y} \end{bmatrix} \begin{Bmatrix} X \\ \gamma_Y \end{Bmatrix} \tag{A1}$$

and

$$\begin{Bmatrix} F_Y \\ M_X \end{Bmatrix} = \begin{bmatrix} k_{11_X} & k_{12_X} \\ k_{21_X} & k_{22_X} \end{bmatrix} \begin{Bmatrix} Y \\ \gamma_X \end{Bmatrix}, \tag{A2}$$

where $k_{11_X}=12EI_X/l^3$, $k_{12_X}=k_{21_X}=6EI_X/l^2$, $k_{22_X}=4EI_X/l$, $k_{11_Y}=12EI_Y/l^3$, $k_{12_Y}=k_{21_Y}=6EI_Y/l^2$, and $k_{22_Y}=4EI_Y/l$.

The area moments of inertia, $I$, are calculated about the $X$ and $Y$ axes. For the uncracked case, the $X$ and $Y$ axes are also the neutral axes of bending.

The asymmetric stiffness relationships are obtained by calculating the appropriate asymmetric area moments of inertia and properly substituting them into the stiffness coefficients $k_{ij}$ above.

The cross section of the shaft at the location of the crack, which is shown in Fig. 10, has asymmetric area moments of inertia about the neutral axes of bending which are parallel to the $X$ and $Y$ axes. To find the area moments of inertia about the neutral axes of bending, the parallel axis theorem was utilized.

The area moments of inertia about the $X$ and $Y$ axes, $\hat{I}_X$ and $\hat{I}_Y$, are defined as

$$\hat{I}_X = \int_A Y^2 dA = \int_A Y^2 dX dY, \tag{A3}$$

$$\hat{I}_Y = \int_A X^2 dA = \int_A X^2 dX dY, \tag{A4}$$

where $A$ is the uncracked area of the cross section. The cross-coupled area moments of inertia, $I_{XY}$ and $I_{YX}$, are zero since the $X$ axis is an axis of symmetry. After integrating over the uncracked area, the following equations for $\hat{I}_X$ and $\hat{I}_Y$ result:

$$\hat{I}_X = \frac{\pi r^4}{8} + \frac{1}{4}\left[(r-a)(r^2-4ra+2a^2)\sqrt{2ra-a^2} + r^4 \sin^{-1}\left(\frac{r-a}{r}\right)\right], \tag{A5}$$

$$\hat{I}_Y = \frac{\pi r^4}{4} + \frac{(r-a)(2\Upsilon)^3}{12} - \frac{1}{4}\left[\Upsilon(2\Upsilon^2-r^2)\sqrt{r^2-\Upsilon^2} + r^4 \sin^{-1}\left(\frac{\Upsilon}{r}\right)\right], \tag{A6}$$

where $r$ is the shaft radius, $a$ is the crack depth, and $\Upsilon = \sqrt{a(2r-a)}$ for convenience.

The following expressions for the area of the cross section, $A$, and the distance from the $X$ axis to the centroid of the cross section, $\overline{X}$, can be obtained

$$A = (r-a)\sqrt{2ra-a^2} + r^2 \sin^{-1}\left(1-\frac{a}{r}\right) + \frac{\pi r^2}{2}, \tag{A7}$$

$$\overline{X} = \frac{2}{3A}(2ar-a^2)^{3/2}. \tag{A8}$$

The moments of inertia about the parallel centroidal axes, $I_X$ and $I_Y$, are then obtained according to the parallel axis theorem as

$$I_X = \hat{I}_X, \tag{A9}$$

$$I_Y = \hat{I}_Y - A\overline{X}^2. \tag{A10}$$

## References


[1] Zou, M., Dayan, J., and Green, I., 2000, "Dynamic Simulation and Monitoring of a Non-Contacting Flexibly Mounted Rotor Mechanical Face Seal," IMechE, Proc. Inst. Mech. Eng. **214**(C9), Part C, pp. 1195–1206.

[2] Lee, A. S., and Green, I., 1994, "Rotordynamics of a Mechanical Face Seal Riding on a Flexible Shaft," ASME J. Tribol., **116**(2), pp. 345–351.

[3] Lee, A. S., and Green, I., 1994, "Higher Harmonic Oscillations in a Noncontacting FMR Mechanical Face Seal Test Rig," ASME J. Vibr. Acoust., **116**(2), pp. 161–167.

[4] Lee, A. S., and Green, I., 1995, "An Experimental Investigation of the Steady-State Response of a Noncontacting Flexibly Mounted Rotor Mechanical Face Seal," ASME J. Tribol., **117**(1), pp. 153–159.

[5] Lee, A. S., and Green, I., 1995, "Physical Modeling and Data Analysis of the Dynamic Response of a Flexibly Mounted Rotor Mechanical Seal," ASME J. Tribol., **117**, pp. 130–135.

[6] Zou, M., and Green, I., 1999, "Clearance Control of a Mechanical Face Seal," STLE Tribol. Trans., **42**, pp. 535–540.

[7] Zou, M., Dayan, J., and Green, I., 1999, "Parametric Analysis of Contact Control of a Noncontacting Mechanical Face Seal," in *Proceedings of Vibration, Noise and Structural Dynamics*, pp. 493–499, April.

[8] Dayan, J., Zou, M., and Green, I., 2000, "Sensitivity Analysis for the Design and Operation of a Noncontacting Mechanical Face Seal," IMechE, Proc. Inst. Mech. Eng. **214**(C9), Part C, pp. 1207–1218.

[9] Zou, M., Dayan, J., and Green, I., 2000, "Feasibility of Contact Elimination of a Mechanical Face Seal Through Clearance Adjustment," ASME J. Eng. Gas Turbines Power, **122**, pp. 478–484.

[10] Dayan, J., Zou, M., and Green, I., 1999, "Contact Elimination in Mechanical Face Seals Using Active Control," in *Proceedings of the IEEE 7th Mediterranean Conference on Control and Automation (MED99)*, pp. 618–619, June.

[11] Tondl, A., 1965, *Some Problems in Rotor Dynamics*, Czechoslovakian Academy of Sciences, Chapman & Hall, London.

[12] Henry, T. A., and Okah-Avae, B. E., 1976, "Vibrations in Cracked Shafts," in *Conference on Vibrations in Rotating Machinery*, pp. 15–19.

[13] Murray, D. B., and McCraith, J. R., 1984, "Vibrational Method for the Detection of Cracks in Rotating Shafts," in *First Parsons International Turbine Conference*, pp. 229–236.

[14] Rao, J. S., 1991, *Rotor Dynamics*, 2nd edition, Wiley, New York.

[15] Gasch, R., 1976, "Dynamic Behavior of Simple Rotor With a Cross-Sectional Crack," in *Conference on Vibrations in Rotating Machinery*, p. 123.

[16] Mayes, I. W., and Davies, W. G. R., 1976, "The Vibrational Behavior of a Rotating Shaft System Containing a Transverse Crack," in *Conference on Vibrations in Rotating Machinery*, pp. 53–64.

[17] Imam, I., and Azzaro, S. H., 1989, "Development of an On-Line Rotor Crack Detection and Monitoring System," ASME J. Vib., Acoust., Stress, Reliab. Des., **111**(3), pp. 241–250.

[18] Huang, S. C., Huang, Y. M., and Shieh, S. M., 1993, "Vibration and Stability of a Rotating Shaft Containing a Transverse Crack," J. Sound Vib., **162**, pp. 387–401.

[19] Tsai, T., and Wang, W., 1998, "Vibration of a Rotor With a Transverse Open Crack," Proc. Natl. Sci. Counc., Repub. China, Part A: Phys. Sci. Eng., **22**, pp. 372–384.

[20] Grabowski, B., 1980, "The Vibrational Behavior of a Turbine Rotor Containing a Transverse Crack," ASME J. Mech. Des., **121**, pp. 140–146.

[21] Dimarogonas, A. D., and Paipetis, S. A., 1983, *Analytical Methods in Rotor Dynamics*, Applied Science.

[22] Herbert, R. G., 1987, "Turbine-Alternator Run-Down Vibration Analysis: Automated Crack Detection," in *11th Biennial Conference on Mechanical Vibration and Noise*, Vol. 2, pp. 631–636.

[23] Inagaki, T., Kanki, H., and Shiraki, K., 1982, "Transverse Vibrations of a General Cracked-Rotor Bearing System," ASME J. Mech. Des., **104**(2), pp. 345–355.

[24] Schmied, J., and Kraemer, E., 1984, "Vibrational Behavior of a Rotor With a Cross-Sectional Crack," in *Conference on Vibrations in Rotating Machinery*, pp. 183–192.

[25] Nelson, H. D., and Nataraj, C., 1986, "The Dynamics of a Rotor System With a Cracked Shaft," ASME J. Vib., Acoust., Stress, Reliab. Des., **108**, pp. 189–196.

[26] Sofker, D., Bajkowski, J., and Muller, P. C., 1993, "Crack Detection in Turbo Rotors, Vibrational Analysis and Fault Detection," in *Conference on Mechanical Vibration and Noise*, Vol. 60, pp. 277–287.

[27] Meng, G., and Hahn, E. J., 1994, "Dynamic Response of a Cracked Rotor With Some Comments on Crack Detection," in *Proceedings of the International Gas Turbine and Aeroengine Congress and Exposition*, June.

[28] Dirr, B. O., and Rothkegel, W., 1994, "Detection and Simulation of Small Transverse Cracks in Rotating Shafts," Arch. Appl. Mech., **64**(3), pp. 206–222.

[29] Inagaki, T., Kanki, H., and Shiraki, K., 1980, "Response Analysis of a General Asymmetric Rotor-Bearing," ASME J. Mech. Des., **102**(1), pp. 147–157.

[30] Dimarogonas, A. D., and Papadopoulos, C. A., 1983, "Vibration of Cracked Shafts in Bending," J. Sound Vib., **91**, pp. 583–593.

[31] Davies, W. G. R., and Mayes, I. W., 1984, "The Vibrational Behavior of a Multi-Shaft, Multi-Bearing System in the Presence of a Propogating Transverse Crack," ASME J. Vib., Acoust., Stress, Reliab. Des., **106**(1), pp. 146–153.

[32] Gasch, R., 1993, "A Survey of the Dynamic Behavior of a Simple Rotating Shaft With a Transverse Crack," J. Sound Vib., **160**, pp. 313–332.

[33] Papadopoulos, C. A., and Dimarogonas, A. D., 1987, "Stability of Cracked Rotors in the Coupled Vibration Mode," in *11th Biennial Conference on Mechanical Vibration and Noise*, Vol. 1, pp. 25–34.

[34] Papadopoulos, C. A., and Dimarogonas, A. D., 1987, "Coupled Longitudinal and Bending Vibrations of a Rotating Shaft With an Open Crack," J. Sound Vib., **117**, pp. 81–93.

[35] Casey, C., 2000, "Crack Detection in Rotor Dynamic System by Vibration Monitoring," M.S. thesis, Georgia Institute of Technology.

[36] Green, I., and Etsion, I., 1986, "A Kinematic Model for Mechanical Seals With Antirotation Locks or Positive Drive Devices," ASME J. Tribol., **108**(1), pp. 42–45.

[37] Tada, H., Paris, P. C., and Irwin, G. R., 1985, *The Stress Analysis of Cracks Handbook*, 2nd Ed., Paris Productions, St. Lous, MO.